EVALUATING REANALYSIS OF VERTICAL CLOUD STRUCTURE

ACROSS A STRATOCUMULUS TO SHALLOW CUMULUS

TRANSITION USING CLOUDSAT-CALIPSO OBSERVATIONS

An Undergraduate Research Scholars Thesis

by

DREW WILLIAM KOERITZER

Submitted to the Undergraduate Research Scholars program at
Texas A&M University
in partial fulfillment of the requirements for the designation as an

UNDERGRADUATE RESEARCH SCHOLAR

Approved by Research Advisor: Dr. Anita D. Rapp

May 2018

Major: Meteorology

TABLE OF CONTENTS

ABSTRACT

Evaluating Reanalysis of Vertical Cloud Structure across a Stratocumulus to Shallow Cumulus
Transition using CloudSat-CALIPSO Observations

Drew W. Koeritzer
Department of Atmospheric Sciences
Texas A&M University

Research Advisor: Dr. Anita D. Rapp
Department of Atmospheric Sciences
Texas A&M University

Stratocumulus clouds play an important role in the global energy balance. Thick layers of stratocumulus clouds over the subtropical oceans gradually thin and transition into shallow cumulus clouds as they traverse from higher latitudes towards the equator. Since these clouds are so widespread, they have a significant radiative effect by reflecting solar radiation, which helps control the cooling of the climate system. Atmospheric reanalyses are uniformly gridded global datasets of atmospheric parameters sourced from historical, current, and model-assimilated observations of the atmosphere. This investigation quantifies the degree to which reanalysis products accurately simulate this cloud regime transition by comparing them to observational satellite data. The physical atmospheric state parameters responsible for reanalysis-observation differences are also identified. Analysis reveals that all reanalysis products exhibit shortcomings in accurately simulating the stratocumulus to cumulus transition, and differences in dynamical and thermodynamical background conditions within each reanalysis environment affect the degree to which each reanalysis depicts cloud coverage and regime type. Understanding errors in model and reanalysis representations of this physical cloud regime transition process will allow researchers to utilize these products with greater awareness of their limitations.

DEDICATION

This work is dedicated to my family, who has always faithfully supported me in my journey to turn a childhood passion into an impactful career.

.

ACKNOWLEDGEMENTS

NOMENCLATURE

CALIPSO   Cloud-Aerosol Lidar and Infrared Pathfinder Satellite

CPR   Cloud Profiling Radar

ERA-Interim European Centre for Medium-Range Weather Forecasts Interim Reanalysis

LTS   Lower Tropospheric Stability

LWC   Liquid Water Content

MERRA   Modern-Era Retrospective Analysis for Research and Applications

NASA   National Aeronautics and Space Administration

SEP   Southeast Pacific Region

SST   Sea Surface Temperature

SECTION I

INTRODUCTION

Stratocumulus clouds cover more of the Earth's surface than any other type of cloud (Warren et al. 1986, Wood 2012). These clouds are characterized by their significant optical thickness (Hahn et al. 2001) leading to notable reflection of shortwave solar radiation (Chen et al. 2000) and as such, they are a crucial component of the global energy balance. Since these clouds are such an integral part of the climate system, the transition from a stratocumulus cloud regime to a shallow cumulus regime with lower overall cloud amounts and less reflection of solar radiation over the southeast Pacific Ocean (SEP) basin is thus a topic of considerable interest. Accordingly, the rate and characteristics of this transition can affect the overall earth albedo and have large consequences on global energy balance. The breakup of thick stratocumulus layers and subsequent transition to shallow cumulus is greatly influenced by various thermal processes (Sandu et al. 2010), including increasing sea surface temperatures (SSTs). In an era of warming climate where accurate in-model characterization of the energy balance is exceptionally important, it is crucial to improve understanding and parameterizations of the atmospheric processes behind this transition to better characterize cloud-climate feedbacks. In Bony and Dufresne (2005), it was noted that vast disagreement regarding the radiative response of tropical clouds to global warming, namely warming SSTs, exists between models. Moreover, it was found that model simulations differ the most, both with future changing climate and with comparisons to current observations, in areas of large-scale subsidence such as the SEP region. Therefore, it is vital to accurately understand and simulate

the stratocumulus clouds common in this region, as it is these low clouds that are responsible for much of the uncertainty surrounding cloud feedbacks within models (Bony and Dufresne 2005).

Stratocumulus clouds are most common over areas with cool SSTs (Klein and Hartmann 1993), particularly along the west coast of subtropical South America, which is the area of focus for this study. This area is particularly favorable for stratocumulus development, due to a relatively shallow and well-mixed boundary layer capped by a strong temperature inversion underneath an area of warm, dry, subsiding air associated with the sinking branches of the Hadley Cell and Walker Circulation (Klein and Hartmann 1993). This air mass is transported from its initial position near the South American coast northwestward towards the equator. As it advects equatorward, the cloud-topped boundary layer encounters warmer SSTs (Sandu et al. 2010) within an environment that is favorable for the boundary layer to alter in a way that supports the gradual breakup of stratocumulus and formation of shallow cumulus (Figure 1) (Wood 2012). As the layer continues to move equatorward, turbulence at the cloud top level
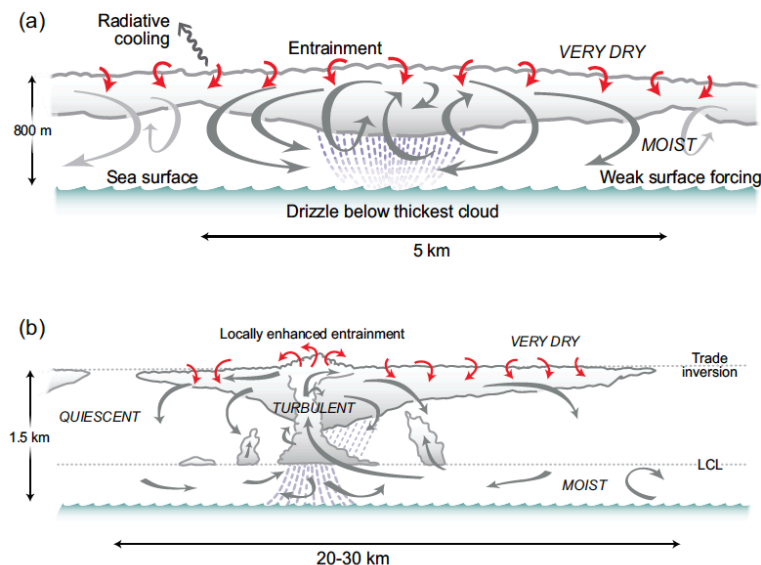

Figure 1. Conceptual diagram illustrating the physical processes influencing the formation and maintenance of a) the well-mixed shallow stratocumulus-topped boundary layer and b) a cumulus-coupled boundary layer in the intermediate stages of transition. Figure from Wood 2012.

drives increased entrainment of warm, dry air into the cloud layer (Bretherton and Wyant 1997), which along with evaporative cooling at the cloud top, helps to increase the inversion height and deepen the boundary layer (Wood 2012). As the boundary layer deepens, it becomes more difficult for the layer to fully mix, which decouples the cloud layer from its source of moisture at the sea surface (Bretherton and Wyant 1997, Wood 2012). Once this decoupling occurs, cumulus clouds driven by energy from the warmer SSTs form below the stratocumulus layer (Wood 2012). As these cumulus clouds deepen, they enhance entrainment of dry air into the stratocumulus layer (Wyant et al. 1997) to the point where the stratocumulus begins to thin and break up. As this process continues, shallow cumulus becomes the dominant cloud type, a point at which overall cloud albedo is significantly reduced from initial values.

With so many physical parameters controlling this transition, their correct representation is crucial to accurately understand this phenomenon and its role in the global energy balance. Observations in the study region over the southeast Pacific are scarce due to remote location and high cost of procurement (Wood and Bretherton 2004); however, data from the National Aeronautics and Space Administration (NASA) Moderate Resolution Imaging Spectroradiometer (MODIS) as well as relatively new data from NASA's A-Train constellation of satellites, specifically from the Cloud Profiling Radar (CPR) aboard CloudSat (Stephens et al. 2002), can now be used to study the physical workings of the cloud regime transition in great detail. Operational since June 2, 2006, the CPR is unique in that it is able to simultaneously detect condensed cloud particles and precipitation in the vertical dimension at a fairly high resolution (Stephens et al. 2008). Launched as the first spaceborne W-band millimeter wavelength radar, the CPR exists to fill gaps in observation of the vertical structure of clouds, and is the first instrument able to retrieve cloud structure and radiative properties at a vertical resolution of

approximately 250 m. In addition, the specific mission focus of CloudSat and the CPR is to improve understanding of the accuracy of the representation of clouds and cloud processes in numerical weather models by means of direct observation (Stephens et al. 2002). As such, data from the CPR is vital to the verification of the reanalysis data analyzed in this study.

Atmospheric reanalyses are common tools used in studies of climate and general atmospheric circulation research (Gelaro et al. 2017). These reanalyses are uniformly gridded global datasets of atmospheric parameters with a numerical model backbone which is used to assimilate observations from many sources. Observations typically have irregular spatial and temporal coverage, and many important atmospheric parameters cannot be directly measured. The embedded numerical model framework is used to extrapolate from the observations and fill in spatial data gaps (Dee et al. 2011). Thus, the main advantage of reanalysis is its continuous uniform grid of atmospheric parameters spanning a large historical time period and the availability of variables that cannot be directly measured but are consistent with observations that do exist. Additionally, many reanalyses are processed to work in near-real time while incorporating historical observations to give a temporally continuous view of global atmospheric circulation patterns for a multi-year period generally beginning in the late 1970s. (Rienecker et al. 2011). Reanalyses are especially useful due to their spatial continuity and representation of both observable and non-observable parameters, and thus are an invaluable tool for climate research (Rienecker et al. 2011, Gelaro et al. 2017). However, most reanalyses have known errors in assimilation and extrapolation due to imperfect model physics and observations; yet, many users regard reanalysis data as essentially equivalent to observations (Dee et al. 2011), an assumption whose validity can be questioned on many fronts.

It is well known that models and reanalysis products have considerable difficulty accurately simulating physical processes and characteristics associated with the stratocumulus to cumulus transition, which can have significant consequences on model representations of cloud-climate feedbacks (Teixeira et al. 2011). Comparing these reanalyses to observations and identifying their errors is an important step as it likely will further increase our understanding of these processes (Wood and Bretherton 2004) and allow for more confident use of reanalysis data in long-term climate studies. Prior studies (Teixeira et al. 2011, Siebesma et al. 2004, Duynkerke and Teixeira 2001, Jakob 1999) have been conducted with a goal of documenting errors in models and reanalysis products related to the simulation of clouds. Specifically, these studies have noted that models and reanalyses can usually capture the interannual variability and rough diurnal cycle of global cloud cover, but are unable to accurately resolve the magnitude of cloud extent. A majority of the attention in these previous studies is given to prior generations of the European Centre for Medium Range Weather Forecasts (ECMWF) reanalysis product and certain climate models, but the broad magnitudes of these errors is likely also present in other models and reanalyses. It is also important to note that many studies focus their analysis on a specific season, usually local summer, or on the diurnal cycle for a relatively short period, with the Teixiera et al. (2011) and Siebesma et al. (2004) analyses only spanning three months in 1998, and a study by Duynkerke and Teixeira (2001) only focusing on a period of one month in 1987. However, these short-term analyses generally exhibit similar conclusions to longer-term studies such as Jakob (1999), which analyzed a period spanning seven years. It has been repeatedly demonstrated that a majority of the model and reanalysis products analyzed consistently underestimate stratocumulus cloud coverage in near-coastal regions, in some cases by as much as 15% compared to observations, while also overestimating clouds in the trade

cumulus regime by as much as 10 to 15% (Jakob 1999). This misrepresentation of clouds

consequently impacts the total radiation budgets simulated by the models, resulting in an

overestimation of downward shortwave radiative flux in stratocumulus regions and subsequent

underestimation in trade cumulus regions. These types of studies, although they are quite broad

and as a result do not allow a very specific diagnosis of the cause of any errors, are useful to

modelers as they generally assist in the refinement of parameterizations and work to improve

overall skill of the model in simulating characteristics of large scale climate.

This basis of this work relies upon a Lagrangian analysis of cloudy parcels as they

transition from stratocumulus to cumulus in the Southeast Pacific (SEP) region. According to

Sandu et al. (2010), this transition is defined as a temporal evolution of overall cloudiness as

individual air parcels travel from higher latitudes toward the equator. The aforementioned study

by Sandu et al. (2010) is an integral component of this work, as it justifies the Lagrangian

perspective used in the forthcoming analysis. In their study, the individual trajectories of

thousands of air parcels undergoing cloud regime transition were calculated using a forward

trajectory model and gridded atmospheric reanalysis data, with each trajectory having a temporal

duration of six days. The composite median (Figure 2) of all calculated trajectories for the SEP
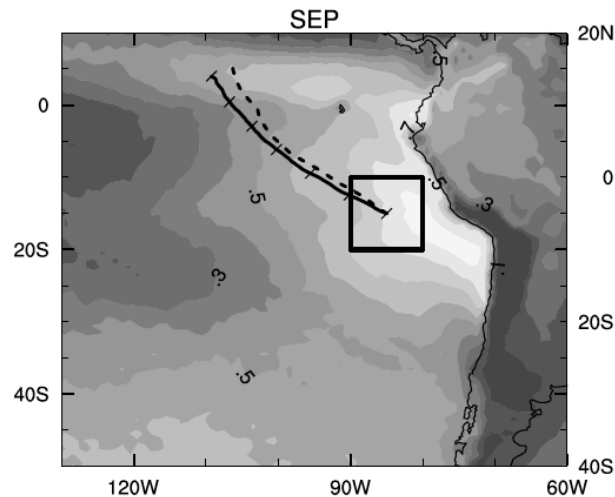

Figure 2. MODIS liquid cloud fraction (contours), median of calculated forward parcel trajectories (solid line), and median of seasonal climatological trajectories (dashed line) in the SEP region. Figure from Sandu et al. 2010.

and other regions was found to be similar to seasonal climatological averages (Sandu et al. 2010). Since the CPR aboard CloudSat is not a scanning instrument and is focused only at nadir, the process of building a suitably large collection of measurements in a given region is quite lengthy. Thus, the results from Sandu et al. (2010) are especially relevant to this study, as they allow for a direct comparison between reanalysis and satellite data through the use of these common climatological trajectory coordinates.

Previous studies (Teixeira et al. 2011, Siebesma et al. 2004, Jakob 1999) have utilized an arbitrarily-defined transect axis on which to conduct their analyses, roughly spanning the meridional extent of the Hadley circulation from the Pacific coast of California to near Hawaii. This axis was used mainly because of its ability to encompass multiple cloud types and include general areas of cloud regime transition. However, this transect is a rough estimate of cloudy parcel trajectory, and its use is only supported by its orientation being close in direction to the mean boundary layer trade wind trajectories extracted from ERA-40 (Teixeira et al. 2011). In addition, these previous studies only analyzed cases in the local summer months, which raises questions regarding the representativeness of the transect and its use in full-year analyses. Here, these concerns are mitigated by compositing observations and reanalysis data along the mean of the individual parcel trajectory from Sandu et al. (2010).

By comparing observational data of cloud features from CloudSat and MODIS with cloud products from atmospheric reanalyses, we aim to understand which reanalysis products best characterize the transition from stratocumulus to cumulus clouds over the southeast Pacific region in a similar style to previous studies. In addition, past studies (e.g. Siebesma et al. 2004) speculate that many differences between reanalysis and observations can be attributed to errors in dynamical process representation. This analysis will attempt to investigate and compare the

11

role of modeled dynamics and thermodynamics in reanalysis in hope of determining which variables drive differences between cloud regime transition within reanalysis compared to observations. Ultimately, we hope this work will help modelers better simulate these sensitive cloud processes, which in turn will improve our overall understanding of how this cloud regime transition impacts the global climate system as a whole.

SECTION II

DATA AND METHODS

This study makes use of three widely-used atmospheric reanalysis data sets available for public use. These include the Modern-Era Retrospective Analysis for Research and Applications (MERRA), Modern-Era Retrospective Analysis for Research and Applications, Version 2 (MERRA-2), both produced by NASA's Global Modeling and Assimilation Office, and the European Centre for Medium-Range Weather Forecasts Reanalysis – Interim (ERA-Interim). MERRA was created with a goal of better integrating global satellite observations since 1979 into a climate context while also improving upon poor representations of the hydrologic cycle found in previous generations of reanalysis (Rienecker et al. 2011). MERRA's data assimilation system ingests over 4 million observations for each 6-hour analysis cycle, many of them sourced from satellite data measuring difficult-to-observe oceanic areas. MERRA-2 was later introduced by NASA as a solution to build upon the strengths of MERRA, while improving in its areas of weakness, namely through the incorporation of additional satellite observations such as additional wind profiler and aerosol data that were not available at introduction of MERRA (Gelaro et al. 2017). The data assimilation scheme and model backbone were also updated in MERRA-2. A notable change to the model physics is the adjustment made to the physical representation of mass in the atmosphere. Specifically, the model within MERRA-2 was updated to reflect the physical assumption that the dry atmospheric mass is unchanging, and any changes in total atmospheric mass are therefore resultant of changes in atmospheric water mass. This is theorized to reduce the occurrence of moisture adjustment within the model which in the past resulted in unrealistic changes in moisture and precipitation fields (Gelaro et al. 2017). The

13

theory behind ERA-Interim is similar to that behind both iterations of MERRA. Similar to

MERRA-2, ERA-Interim incorporates the updated theory regarding consistent atmospheric dry

mass which has general implications for improving representation of moist processes within the

boundary layer (Dee et al. 2011). Notably, this updated atmospheric mass scheme results in

increased production of stratocumulus clouds within ERA-Interim in previously

underrepresented areas, including in the SEP region. As is the case with other reanalyses, it is

important to evaluate this in the context of observational satellite data to confirm improvements.

Since various cloud properties are not directly observed, the model backbone within each

reanalysis is responsible for processing raw observations into meaningful cloud products, and it

is the different execution of this step which results in differences between various reanalyses. All

reanalysis data used in this study was extracted as time- and instantaneously-averaged monthly

means for the SEP region bounded by longitudes -110.625° to -64.375° and latitudes -35.625° to

5.625° for the period from January 2007 to December 2010, resulting in a total of 48 months of

data that overlaps with the period of CloudSat observations.

Table 1: Specifications of model reanalyses used in this study.

	Horizontal Resolution	Cloud Variables	State Variables
MERRA	1.25° x 1.25°	Cloud Fraction for Radiation (3d) Cloud Liquid Water Content (3d) Total Cloud Fraction (2d) Low Cloud Fraction (2d)	Temperature Specific Humidity Vertical Pressure Velocity Potential Temperature
MERRA-2	0.625° x 0.5°	Cloud Fraction for Radiation (3d) Cloud Liquid Water Content (3d) Total Cloud Fraction (2d) Low Cloud Fraction (2d)	Temperature Specific Humidity Vertical Pressure Velocity Potential Temperature
ERA-Interim	0.75° x 0.75°	Cloud Fraction (3d) Cloud Liquid Water Content (3d) Total Cloud Fraction (2d) Low Cloud Fraction (2d)	Temperature Specific Humidity Vertical Pressure Velocity Potential Temperature

The trajectory of an air parcel undergoing stratocumulus to cumulus transition is defined

using the coordinates given in Sandu et al. (2010) as the climatological average for parcels

undergoing the transition within the SEP region. The coordinates along the trajectory are not

evenly spaced, and the grid output and spacing of the three reanalyses differ from each other and

with the trajectory coordinates. To define the specific reanalysis grid coordinates along which to

conduct our analysis, a grid was defined according to the native resolution of each reanalysis.

Points within each grid along the linear segment between each coordinate from Sandu et al.

(2010) were used as the trajectory coordinates for all products extracted from that reanalysis.

This resulted in slightly different trajectory coordinates for each reanalysis; however, points

along each trajectory are only separated by small distances, illustrated in Figure 3. However, this
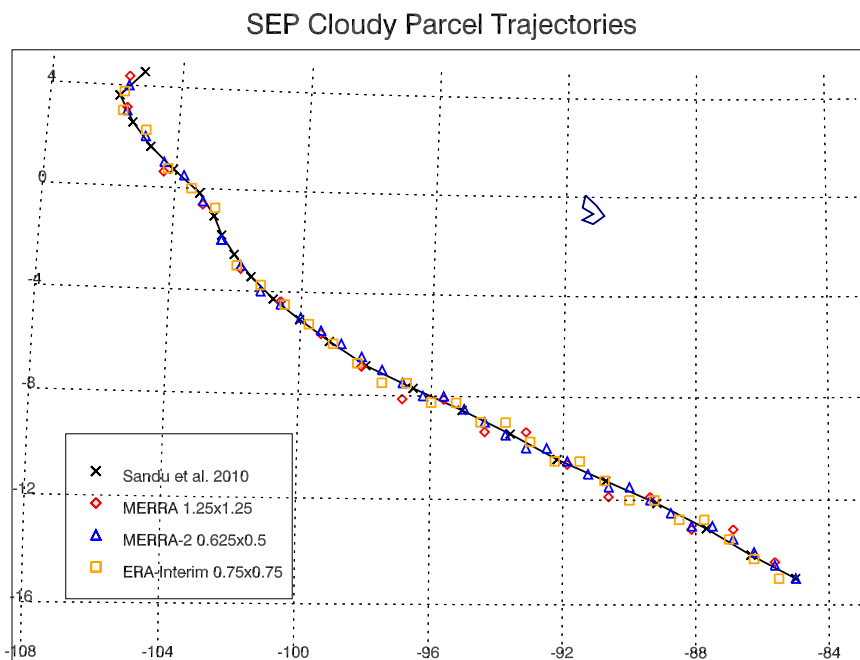

Figure 3. Coordinates along transition trajectories used for analysis of MERRA, MERRA-2, and ERA-Interim, compared to the climatological coordinates given in Sandu et al. (2010)

approach to resolution matching does produce some mild roughness in data continuity, especially

in vertical profile plots, since the coordinates were chosen based on a nearest-neighbor approach

and the data for each reanalysis was not interpolated to a common grid resolution. Areal cloud

fraction data were extracted in two dimensions at native grid resolution for all reanalyses, and

cloud fraction for radiation data along with atmospheric state variable data were extracted in

15

three dimensions at grid resolution, with standard atmospheric pressure levels from 1000 hPa to 100 hPa as vertical coordinates. All data were extracted as time- and instantaneously-averaged monthly averages for the 48-month period from January 2007 to December 2010. These data were then averaged temporally to provide mean values representative of the entire three-year period from 2007 to 2010.

To illustrate broad large-scale cloud patterns within each reanalysis product in a conceptual manner similar to what a satellite sensor would observe looking downwards at the earth, two-dimensional areal cloud fraction for the entire SEP region was overlaid on a map along with respective trajectory coordinates. The 2-d reanalysis map products were then compared with observational data from MODIS extracted from Zapalac (2014), which was mapped using a similar procedure to provide an initial direct comparison between reanalysis depictions and observations for the same period. Precise cloud fraction data values along the overlain transition trajectory were then extracted and plotted as a series of line plots with the latitude as x-coordinate, allowing the line plots to serve as a time series proxy for the entire transition period as the cloudy parcels move equatorward. This comparison was performed with a goal of more directly evaluating the evolution of vertical cloud structure and overall cloud regime through time.

The CPR aboard CloudSat allows for a very detailed view into the vertical structure of clouds within its field of view. The CPR provides a higher degree of detail about clouds and precipitation compared to previous instruments such as those used during the Tropical Rainfall Measurement Mission (TRMM). Consequently, the CPR is immensely useful in the context of this study, as it provides high-resolution information on vertical structure and characteristics within clouds. Operating at a 94 GHz frequency with a 3.3 μs pulse length and 1.85 m diameter

antenna, the CPR can resolve measurements at a 250 m vertical resolution within a 1.4 x 3.5 km field of view (Stephens et al. 2002). To visualize reanalysis output in a manner similar to what is possible with CloudSat products, three-dimensional cloud fraction for radiation was plotted as a vertical cross section with latitude coordinates along the transition trajectory serving as abscissa and height above sea level as the ordinate. Height was limited from zero to approximately 3000 m above the surface due to the limited vertical extent of subtropical stratocumulus and trade cumulus clouds, and to limit focus to within and just above the marine boundary layer. Cloud liquid water content (LWC) was also plotted as a vertical cross section along the transition trajectory to determine how well reanalysis products are able to capture the cloud water variability across the transition. CloudSat data and figures used in this analysis are provided from Zapalac (2014).

Since the broad focus of this study is to evaluate and diagnose the source of error in reanalysis of cloud regime transitions, several physical atmospheric state variables were also plotted as vertical cross sections along the transition trajectory. This type of comparison was performed to contribute to the fundamental goal of determining the relative importance of dynamic and thermodynamic influences within models in affecting representation of cloud properties and timing of cloud regime changes. For each reanalysis, temperature, relative humidity, specific humidity, and vertical pressure velocity (ω) were plotted as vertical profiles along the aforementioned transition trajectories, both in height coordinates from 0 to 3000 m above the surface to capture differences in the vicinity of the boundary layer, and in pressure coordinates from 1000 to 100 hPa to obtain a more complete picture of the atmospheric column. In addition to the standard variables mentioned above, lower tropospheric stability (LTS) was calculated in the same manner as in Klein and Hartmann (1993) as a proxy for inversion strength

by computing the difference between potential temperature at 700 hPa and at 1000 hPa (LTS = $\theta_{700} - \theta_{1000}$). To quantify the variation between each reanalysis depiction of the dynamical and thermodynamical structure of the atmosphere along the transition trajectory, the numerical difference of each state variable between MERRA-2 and both MERRA and ERA-Interim was calculated for all grid points. MERRA-2 was chosen as the reference due to its relatively recent introduction in comparison to the other two products. However, due to differences in grid spacing and the resulting slightly different specific trajectory coordinates, the data was interpolated to perform comparisons at consistent coordinates. To maximize simplicity, the highest resolution reanalysis, MERRA-2, was interpolated to match the lower resolution grids of MERRA and ERA-Interim. To do this, the nearest matching coordinate in MERRA-2 to each trajectory coordinate in MERRA and ERA-Interim was identified, and the MERRA-2 data was then interpolated from its native grid resolution to obtain the data value at the coordinate of the lower-resolution reanalysis. In this way, it was possible to calculate direct differences between the reanalyses, and thus diagnose the general dynamic and thermodynamic differences between each reanalysis along the transition trajectory, and identify possible shortcomings in each reanalysis.

To finalize the analysis and illustrate the importance of accurate simulation of clouds in reanalysis, cloud shortwave radiative forcing at the top of the atmosphere was calculated for each reanalysis by taking the difference between the top-of-atmosphere net shortwave radiation and top-of-atmosphere net shortwave radiation assuming only clear skies. This metric allowed for simple quantification of the effect of varying cloud production within reanalysis in terms of overall large scale radiative effects.

SECTION III

RESULTS

    The results shown in this section all are from the 48-month period between January 2007 and December 2010, with sourced data representing the SEP region bounded by the coordinates mentioned previously. Initial comparison of 2-d areal cloud fraction for each reanalysis reveals modest similarities in patterns of cloud distribution over the SEP region for each. However, these
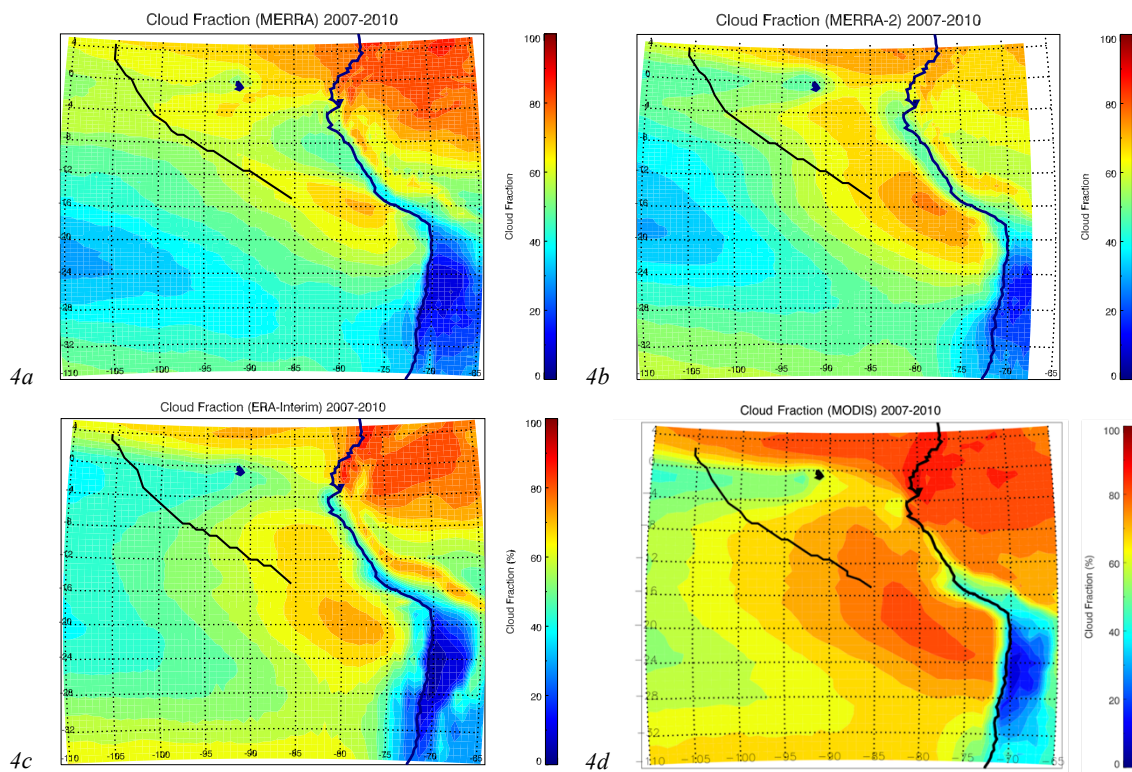

Figure 4. 2-d areal cloud fraction (contours) and transition trajectory (black line) for MERRA (a), MERRA-2 (b), ERA-Interim (c), and MODIS (d). Figure 4d from Zapalac 2014.

figures illustrate the inconsistencies in total cloud fraction between each reanalysis, and provide an overview of the problem at hand. Namely, while all reanalyses generally simulate approximately 70% cloud fraction at the start of each trajectory, they differ in speed of the transition, with ERA-Interim (Figure 4c) clearly reducing cloud fraction along the trajectory

much more quickly than MERRA (Figure 4a) and MERRA-2 (Figure 4b). MERRA and

MERRA-2 both also exhibit an overall lower magnitude of cloud fraction throughout the SEP

region compared to ERA-Interim, although it is clear that the improvements made to MERRA-2

resulted in a net increase in overall magnitude of simulated cloud fraction. In general, the plots in

Figure 4 suggest that ERA-Interim has a larger change in cloud fraction across the stratocumulus

to cumulus transition than both iterations of MERRA, illustrated through the reduction in cloud

fraction along the trajectory at latitudes north of approximately -10°, which can be seen clearly in

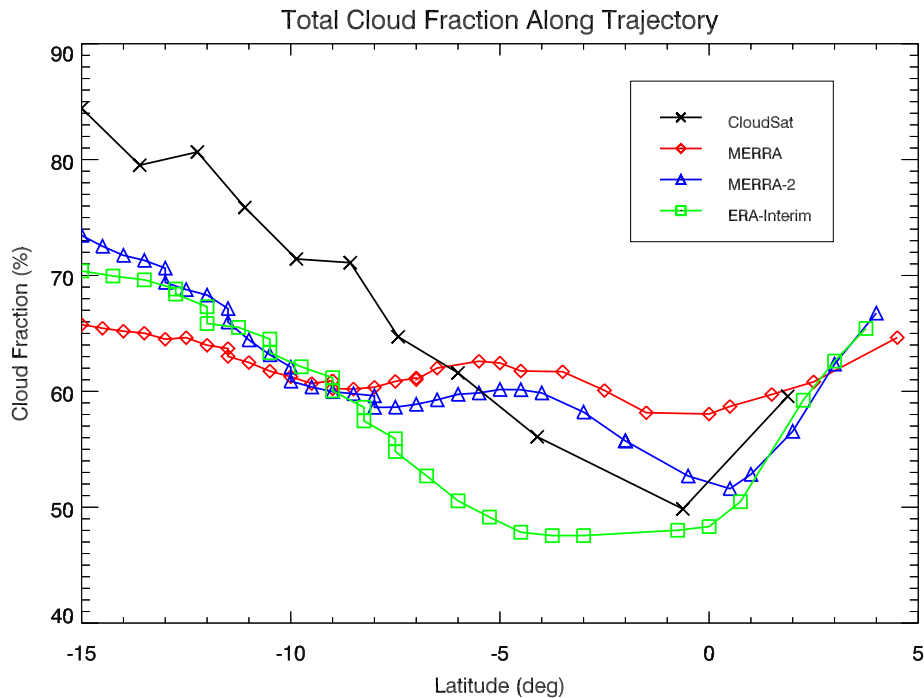Figure 5. In addition, the rate of cloud fraction decrease in ERA-Interim is similar to that

Figure 5. Comparison of areal cloud fraction values for CloudSat and for each reanalysis along its respective transition trajectory.

observed by CloudSat. However, it is clear that in comparison to observational MODIS (Figure

4d) and CloudSat (Figure 5) data, all reanalyses produce cloud fraction values that are too small

throughout most of the SEP region. The difference between the reanalyses and MODIS is most

evident in the near-coastal regions west of South America, where reanalysis products generally

under-simulate cloud fraction by 10 to 20%. Along the trajectory, MODIS observes a slow

decrease in cloud fraction at higher latitudes, followed by a more rapid decrease in the vicinity of

the equator. CloudSat observes a similar decrease in cloud fraction, although the rate of decrease

along the trajectory is consistent until a minimum in cloud fraction is observed near the equator.

While no reanalysis product matches this observed transition pattern exactly, ERA-Interim

produces cloud fraction values along the trajectory in a pattern similar to MODIS and CloudSat,

with the rate of decrease in cloud fraction in ERA-Interim very similar to the rate observed by

CloudSat. However, ERA-Interim produces too few clouds overall, especially in far eastern and

southern regions of the SEP compared to MODIS. MERRA under-simulates cloud fraction at

higher latitudes and over-simulates it along the trajectory near the equator, and while MERRA-2

has a somewhat more realistic pattern compared to MODIS and CloudSat near the equator, it still

under-simulates cloud fraction at higher latitudes.

Three-dimensional cloud fraction for radiation was plotted as a vertical cross section

along the transition trajectory for each reanalysis, shown in Figure 6a-c. This was completed

with a goal of analyzing the differences in vertical structure and representation of cloud fraction

in each reanalysis compared to observational data from CloudSat, shown in Figure 6d. It is quite

obvious that CloudSat-observed cloud fraction values are significantly higher than those present

in all reanalyses. Fundamentally, these large discrepancies are caused by differences in how

cloud fraction is physically defined in reanalysis products and observational datasets such as

CloudSat. According to Brooks et al. (2005), many atmospheric circulation models, including

reanalyses, define three-dimensional cloud fraction in terms of the volume of each vertical grid

box filled with cloud (C_v) for the purposes of calculating radiative effects of clouds. Contrarily,

many observational products, including those from CloudSat used in this study, define cloud
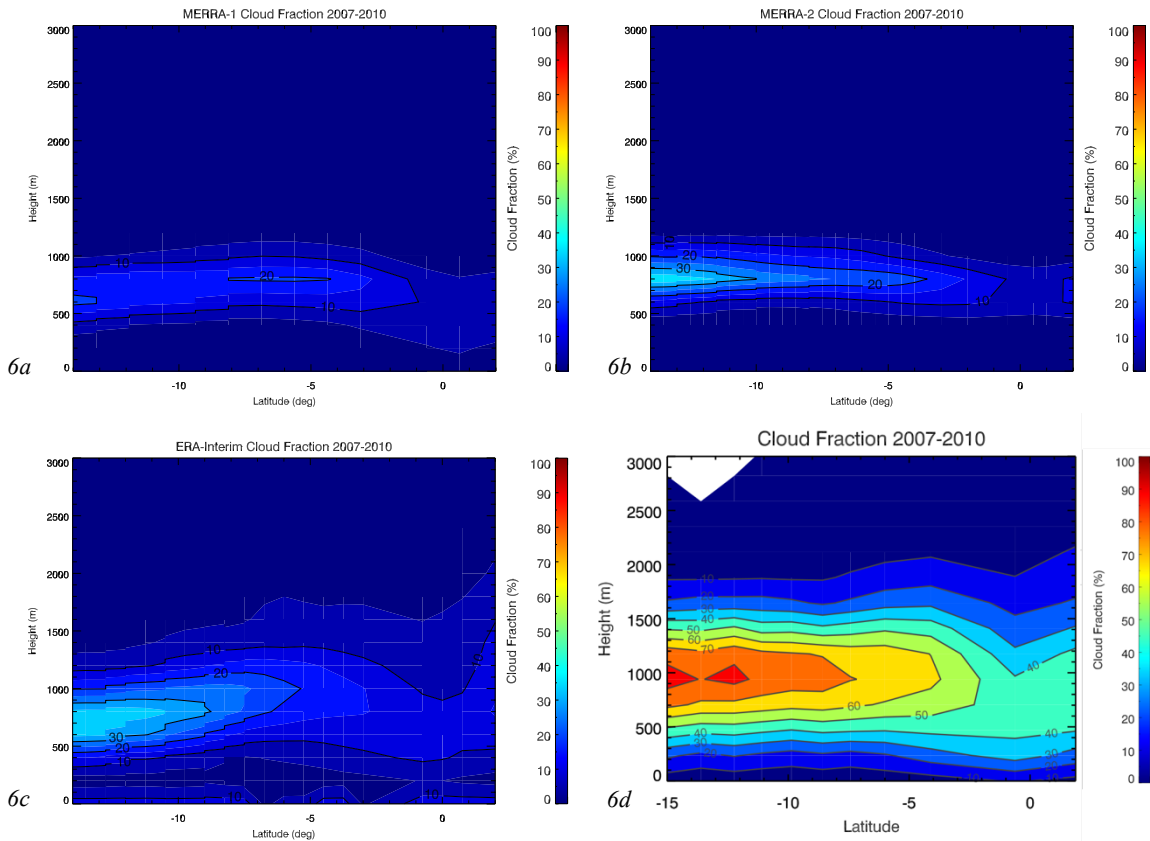
21

Figure 6. Vertical cross section of cloud fraction along the transition trajectory for MERRA (a), MERRA-2 (b), ERA-Interim (c), and CloudSat (d). Figure 6d from Zapalac 2014.

fraction in terms of area of the top of a vertical grid box that is covered with cloud (C_a). This

distinction is shown in Figure 7. Brooks et al (2005) also note that by definition, C_a will always

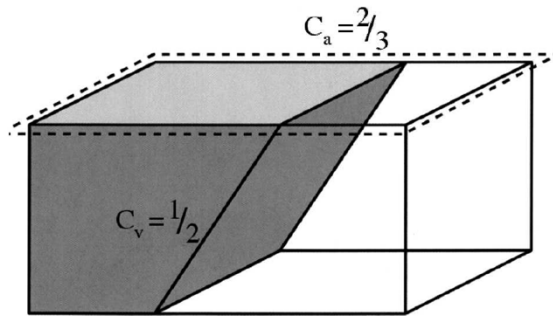be greater than or equal to C_v, which explains the significantly higher cloud fraction values seen

Figure 7. Schematic representation of the difference between three-dimensional cloud fraction by volume (C_v) and cloud fraction by area (C_a). Figure from Brooks et al. 2005.

by CloudSat. Furthermore, this also means that the magnitude of cloud fraction from CloudSat is

not directly comparable to the magnitude of vertical cloud fraction produced by each reanalysis,

and a parameterization is required to convert C_v into a quantity directly comparable to C_a, which was not completed as part of this study. Despite the incomparability of the magnitude of cloud fraction between observations and reanalysis, the general vertical structure of the cloud layer in each reanalysis can be compared to the structure seen by CloudSat. Most notably, at lower latitudes, observational CloudSat data reveals increasing depth of clouds, as larger cloud fraction values extend both higher above initial levels and further below them towards the surface. While MERRA and MERRA-2 seem to keep vertical cloud depth rather consistent along the entire trajectory, ERA-Interim is similar to observations in that it simulates increasing vertical cloud extent higher into the atmosphere at lower latitudes.

Due to the fundamental differences between areal and volume-derived cloud fraction between observations and models described above, cloud liquid water content (LWC) was also
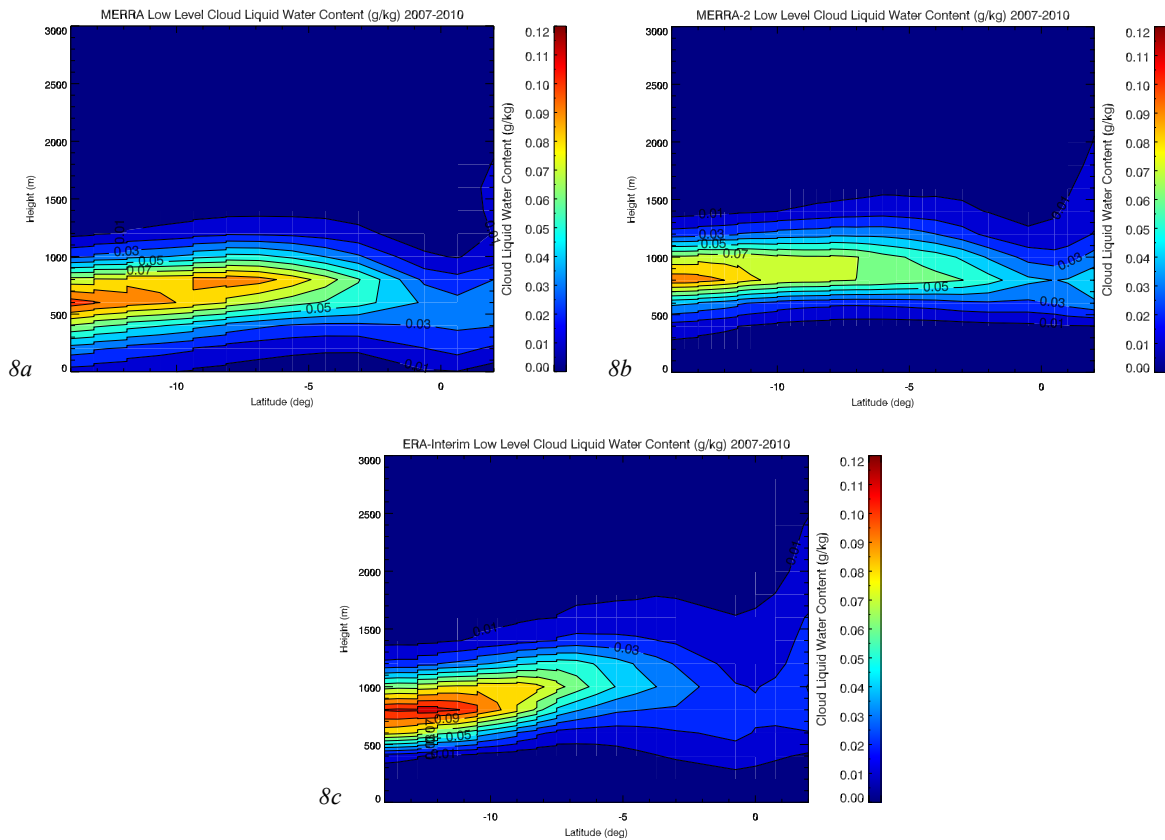

Figure 8. Cloud liquid water content along the transition trajectory for MERRA (a), MERRA-2 (b), and ERA-Interim (c).

23

analyzed (Figure 8a-c) for comparison of cloud structure along the transition trajectory for each reanalysis. Within the SEP region and along the trajectory, vertical cloud extent is overall quite limited, with clouds mainly confined to the marine boundary layer. To obtain maximum detail for analysis, LWC was plotted from the surface to 3000 m above sea level, highlighting the vicinity of the boundary layer as the focus of this portion of the analysis. For all reanalysis products, LWC exhibits a maximum in the layer between 500 and 1000 m above sea level. ERA-Interim (Figure 8c) produces the highest LWC values of all reanalyses at latitudes between -15° and -10°, while MERRA-2 (Figure 8b) produces the smallest magnitude of LWC at this point. MERRA (Figure 8a) produces its maximum of LWC about 100 to 200 meters lower in altitude than both MERRA-2 and ERA-Interim. As the cloudy parcels move equatorward along the trajectory, LWC maxima in both MERRA and ERA-Interim rise gradually in altitude, peaking in altitude at approximately -7° latitude. This contrasts with MERRA-2, which keeps LWC maxima at a nearly consistent altitude throughout the transition. MERRA-2 and ERA-Interim restrict notable LWC values to altitudes above about 500 meters, while MERRA simulates non-negligible LWC values much closer to the surface. In addition, ERA-Interim simulates a relatively fast decrease in LWC, with the transition to significantly lower values than both MERRA and MERRA-2 occurring quite early along the trajectory. MERRA-2 retains elevated LWC values for a longest of all reanalysis products. These trends imply rather significant differences between the reanalyses in terms of cloud structure along the transition trajectory. ERA-Interim produces the thickest cloud layer at higher latitudes, followed by MERRA, with MERRA-2 producing the most vertically-limited cloud deck at high latitudes. Also at the beginning of the transition trajectory, MERRA-2 and ERA-Interim exhibit mostly clear skies below approximately 500 m, while MERRA produces notable amounts of cloud water below this

in the vicinity of the surface. This indicates that the boundary layer is likely being physically resolved differently in MERRA than in MERRA-2 or ERA-Interim, suggesting that MERRA is either simply producing much lower boundary layer top heights than the other reanalyses or is not isolating cloud water at the top of the boundary layer as seen in MERRA-2 and ERA-Interim. However, the increasing altitude of maximum simulated LWC during the transition in both MERRA and ERA-Interim do imply a subtle rising of the inversion height and subsequent deepening of the boundary layer towards the middle of the transition trajectory. This trend matches well with the conceptual physical models of the transition described in previous literature, but is absent in MERRA-2. As the transition continues at higher latitudes, ERA-Interim seems to best capture the dominant cloud regime shifting from stratocumulus to cumulus, implied by steady decrease in LWC and more extensive vertical presence of non-negligible LWC values, consistent with cumulus beginning to penetrate the top of the boundary layer, assisting in the breakup of the stratocumulus. While the decrease in overall LWC values is indeed present in MERRA and MERRA-2, it is a much more gradual decrease, and there is a smaller increase in vertical extent of cloud water, suggesting that both iterations of MERRA are able to simulate decreasing overall cloud coverage, but may not be capturing the dominant cloud regime transition to more vertically-towering cumulus.

To better understand how the environment of each reanalysis shapes the transition from stratocumulus to cumulus in each reanalysis, a lower tropospheric stability (LTS) index originally defined by Klein and Hartmann (1993) (LTS = $\theta_{700\,hPa}$ - $\theta_{1000\,hPa}$) was calculated and used as a proxy to assess inversion strength, and is useful in estimating the ability of cumulus to effectively penetrate above the boundary layer into the free troposphere At the initial beginning of the trajectory, all reanalyses exhibit similar values of LTS (Figure 9). As the trajectory moves

equatorward, LTS gradually decreases, with MERRA and MERRA-2 only varying from each

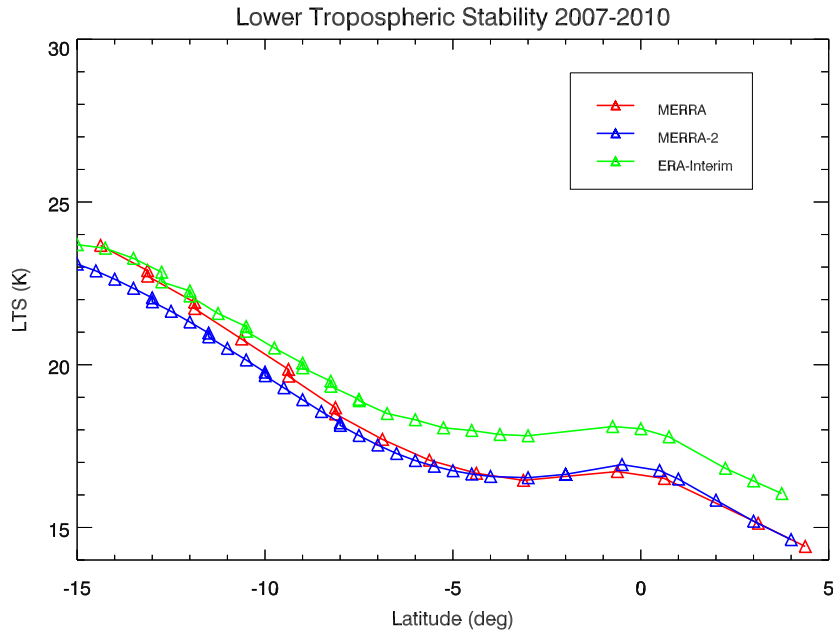other by a maximum of approximately 1 K. LTS within ERA-Interim is appreciably higher than

Figure 9. Lower tropospheric stability for all reanalysis products along the transition trajectory.

both iterations of MERRA, beginning at about -10° latitude and continuing throughout the

remainder of the trajectory. Physically, the higher values of LTS within ERA-Interim would

suggest a stronger inversion at the top of the boundary layer, resulting in a theoretically stronger

barrier to developing cumulus clouds. However, this is disputed by LWC profiles, which suggest

that despite higher LTS and a resulting stronger inversion, ERA-Interim still simulates increasing

vertical cloud extent. This suggests that large-scale dynamical or thermodynamical factors may

also be related to the cloud regime transition differences.

To further explore the possible effects of various dynamical and thermodynamical

environmental variables and patterns of cloud regime transition, several of these variables,

including temperature, specific humidity, and vertical pressure velocity (ω), were plotted along

the transition trajectory. These variables as produced by MERRA-2 are shown in Figures 10, 11,

and 12, respectively. Within the temperature profile shown in Figure 10, a temperature inversion

is notably present at about 1500 m from the beginning of the trajectory until about -5° latitude. The inversion gradually weakens along the trajectory, beginning with a strength of about 4 K which decreases steadily until the inversion dissipates at lower latitudes. This weakening
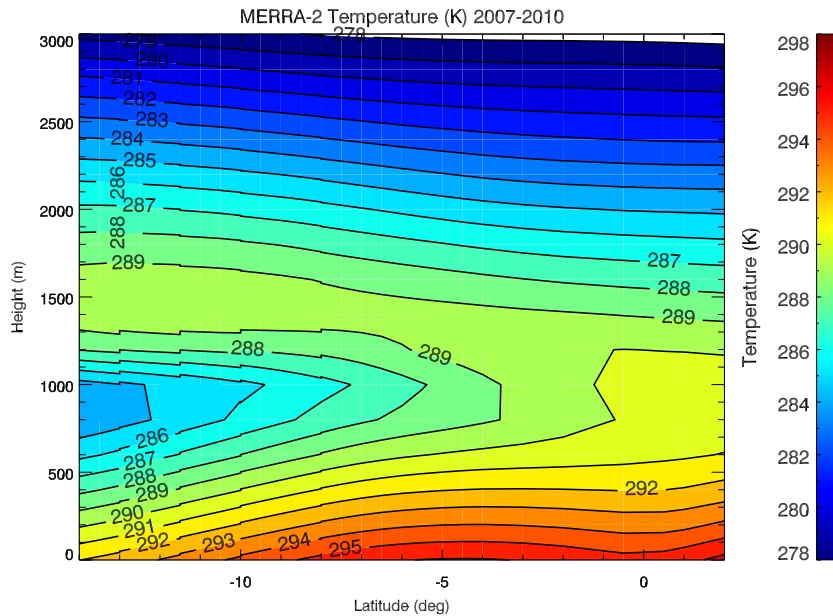

Figure 10. Temperature along the MERRA-2 transition trajectory, from the surface to 3000 m above sea level.

temperature inversion corresponds to a steady decrease in LTS, which is reflected in Figure 9, therefore allowing for easier vertical growth of cumulus and reduction of the main thermodynamical limit on cloud regime change. Analysis of the specific humidity profile shown in Figure 11 reveals a sharp decrease in specific humidity between 750 and 1250 m above the surface at the beginning of the trajectory. As the trajectory continues equatorward, the vertical gradient of specific humidity decreases in magnitude, with overall higher specific humidity values and a less stratified, more uniform vertical profile as specific humidity decreases with height. The dry environment and associated low specific humidity above approximately 1250 m near the beginning of the trajectory is consistent with the subsiding air associated with the sinking branch of the Hadley circulation at these relatively high latitudes, which further reinforces the temperature inversion at the top of the boundary layer. This is further confirmed
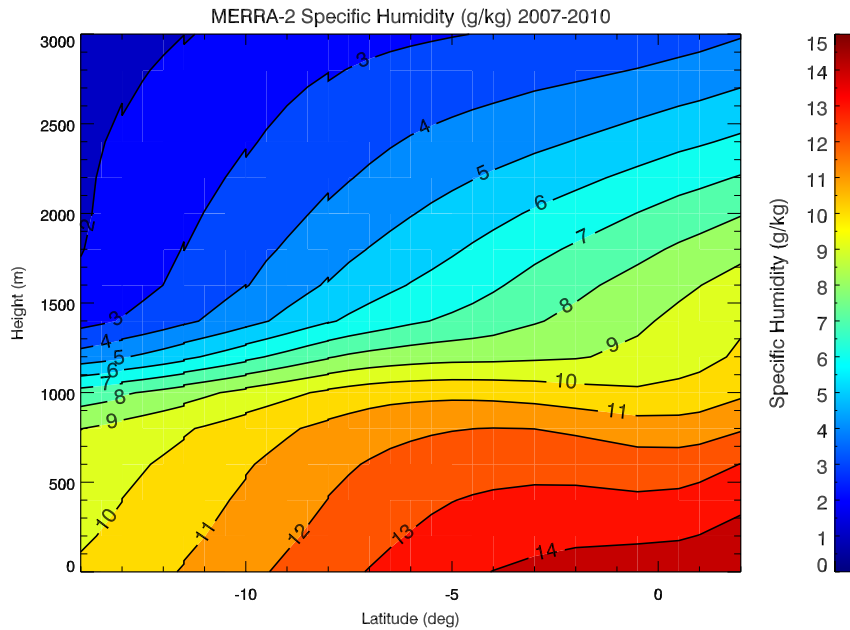
27

Figure 11. Specific humidity along the MERRA-2 transition trajectory, from the surface to 3000 m above sea level.
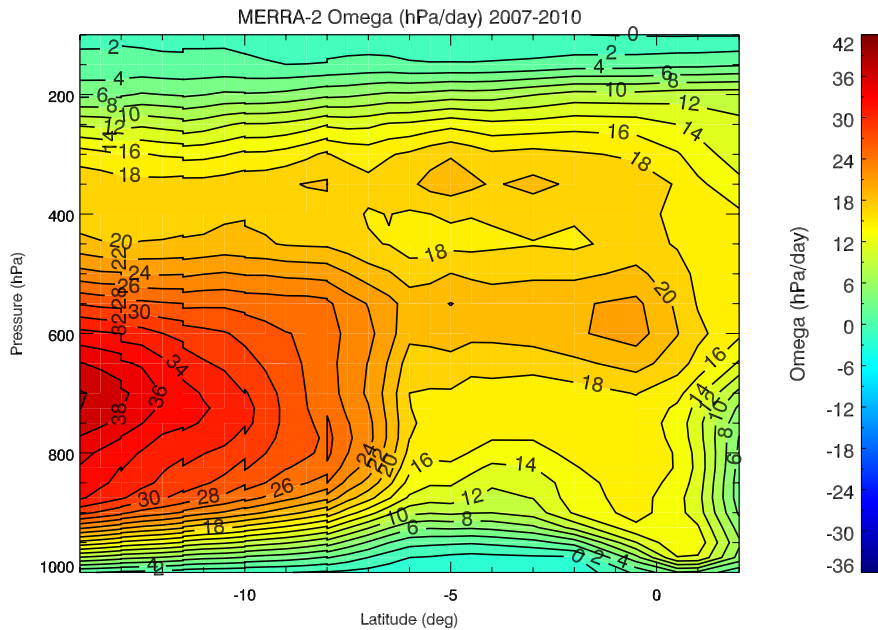

Figure 12. Vertical pressure velocity along the MERRA-2 transition trajectory, from 1000 hPa to 100 hPa.

by the ω profile shown in Figure 12. This large-scale view of ω throughout most of the

atmospheric column highlights the strong subsidence at midlevels near the beginning of the

trajectory, supporting the low specific humidity and strong temperature inversion in this area. As

the trajectory moves equatorward, subsidence weakens considerably, but is notably still present

throughout most of the column. However, the weakening of the subsidence and its correspondence with the weakening temperature inversion and reduction in stratification of specific humidity suggest that subsidence alone is unable to stifle cloud regime transition, and the modification of the thermodynamic and moisture profiles is enough to allow for marginal cloud regime transition at lower latitudes in MERRA-2.

To better visualize and understand the subtle differences in these variables between reanalysis products, these differences were plotted, using MERRA-2 as the reference. By analyzing the differences in state variable fields between the reanalyses, the patterns and differences observed in each reanalysis depiction of clouds along the trajectory can be put into the context of the background dynamic and thermodynamic environment, which will aid understanding of how various fields within each reanalysis affect their depiction of the cloud regime transition. The difference in temperature, specific humidity, and ω between MERRA-2 and MERRA are shown in Figure 13, 14, and 15, respectively. From these figures, it can be seen that the largest differences between the two iterations of MERRA occur in the area near and above the boundary layer at mainly the beginning of the transition trajectory. When analyzing the temperature differences in Figure 13, it is clear that MERRA-2 produces a stronger temperature inversion than MERRA. The top of the boundary layer at about 1000 m above sea level is approximately 2 K cooler in MERRA-2 than in MERRA, with the above temperature inversion about 1 K warmer than in MERRA. Within the specific humidity difference profile (Figure 14), the majority of the discrepancies in specific humidity between MERRA and MERRA-2 are also mainly confined to the beginning of the trajectory. MERRA-2 resolves more moisture at the top of the boundary layer centered at about 1000 m above sea level, while MERRA-2 is drier immediately above the top of the boundary layer. This corresponds quite well
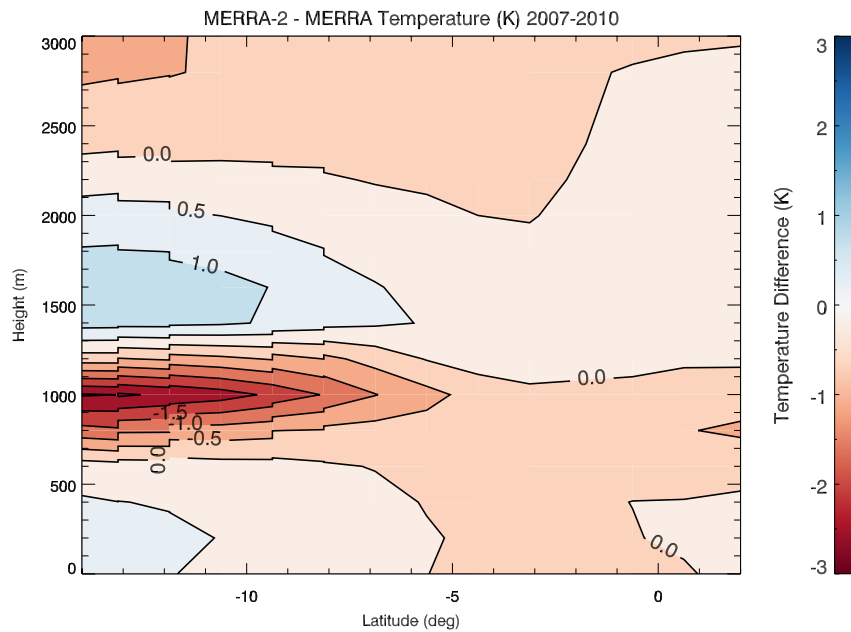
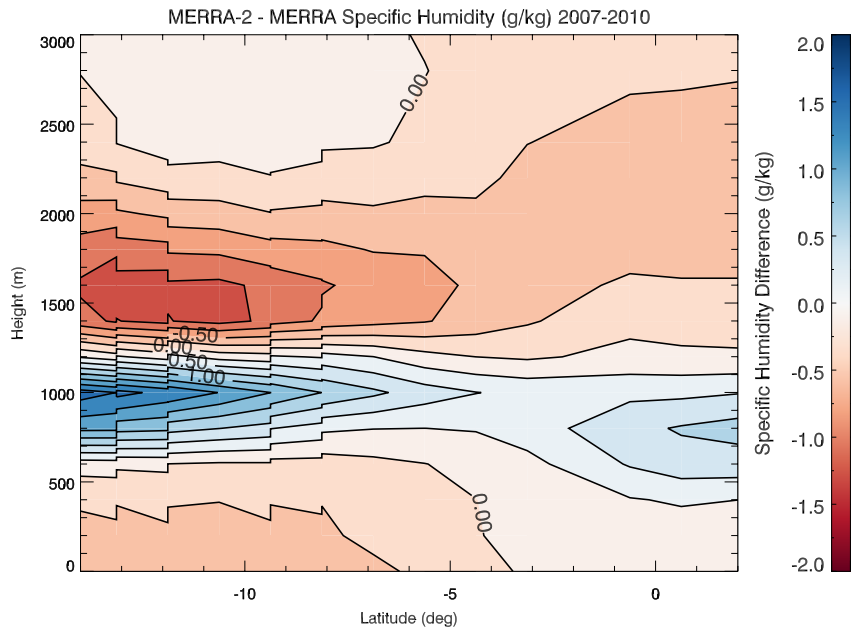*Figure 13. Difference in temperature between MERRA-2 and MERRA.*

Figure 14. Difference in specific humidity between MERRA-2 and MERRA.

to the differences observed in the temperature profile, which were also centered in the vicinity of

the top of the boundary layer. The reasoning for this similarity in pattern is revealed upon

analysis of the differences in ω between MERRA and MERRA-2 in Figure 15. At the beginning

of the trajectory, MERRA-2 produces notably stronger subsidence at midlevels, which

corresponds to a larger temperature inversion at the top of the boundary layer and more

stratification in the specific humidity field. While the similarities in patterns between the
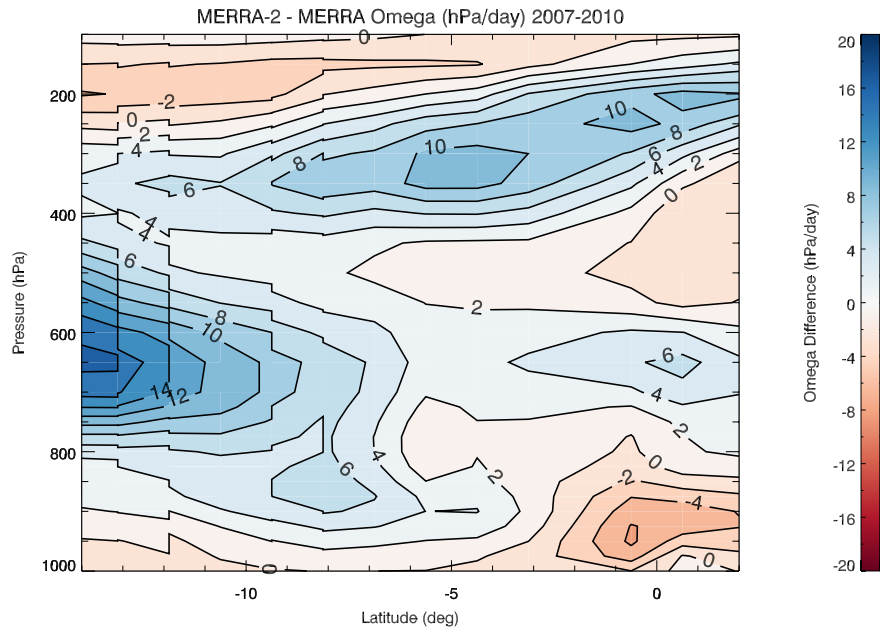

Figure 15. Difference in vertical pressure velocity between MERRA-2 and MERRA.

difference plots are notable, despite these differences, the evolution of cloud regime and vertical

structure as seen in the LWC profiles for both MERRA and MERRA-2 in Figure 8 is still quite

similar, although a slightly deeper boundary layer in MERRA-2 than in MERRA may be

responsible for the lack of cloud water so close to the surface in MERRA-2.

The difference in temperature, specific humidity, and ω between MERRA-2 and ERA-

Interim are shown in Figures 16, 17, and 18, respectively. Studying the temperature difference

between the two reanalyses, it is evident that MERRA-2 produces a slightly stronger temperature

inversion at the top of the boundary layer, implied by lower temperatures than ERA-Interim at

about 1000 m above sea level, and slightly warmer temperatures than ERA-Interim at about 1500

m above sea level. Interestingly, this stronger inversion in MERRA-2 is carried along the

trajectory until about -3° latitude, which is quite a bit farther than the inversion differences are

carried in the comparison of MERRA-2 with MERRA. This potentially suggests the reason that

ERA-Interim more obviously simulates the increasing vertical extent of clouds in the near-

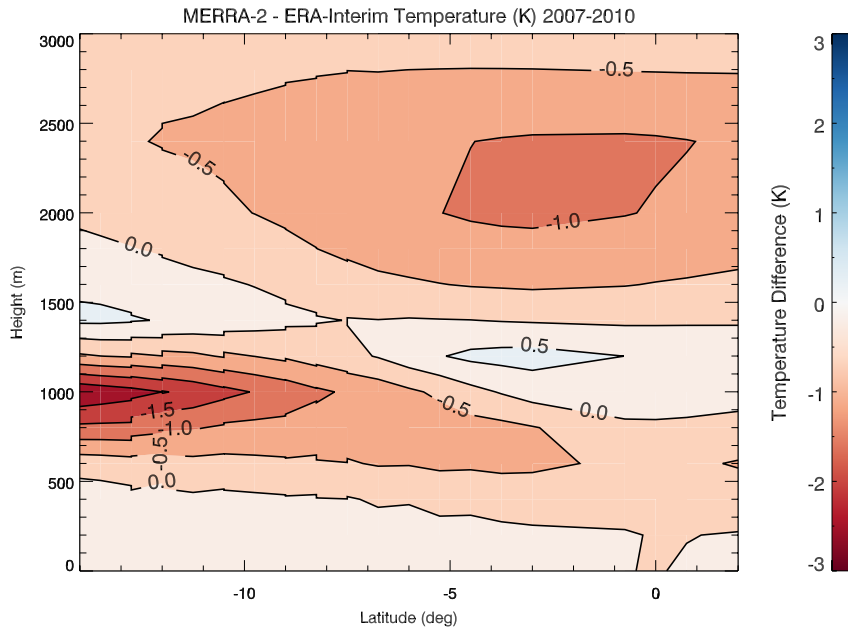equatorial latitudes of the trajectory; namely, because ERA-Interim features a weaker inversion

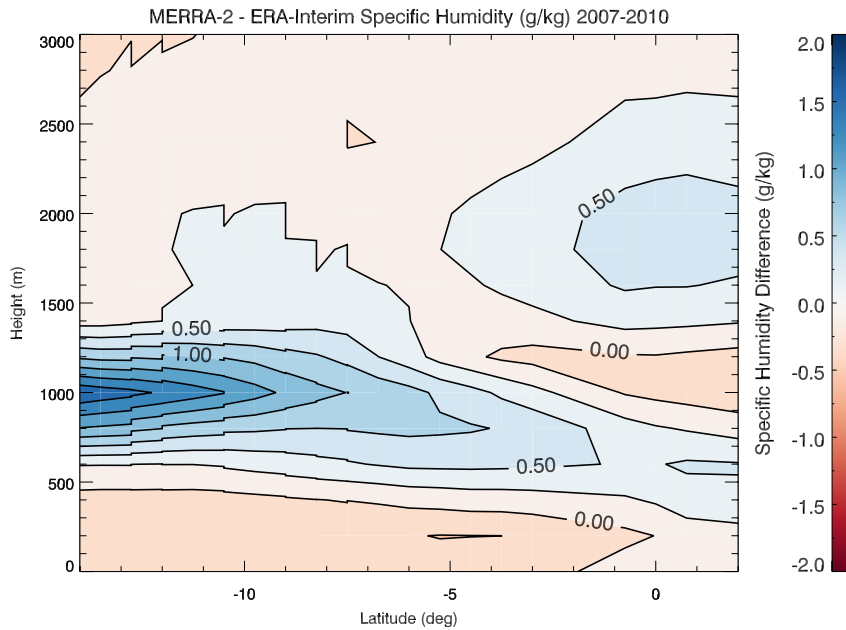*Figure 16. Difference in temperature between MERRA-2 and ERA-Interim.*

Figure 17. Difference in specific humidity between MERRA-2 and ERA-Interim.
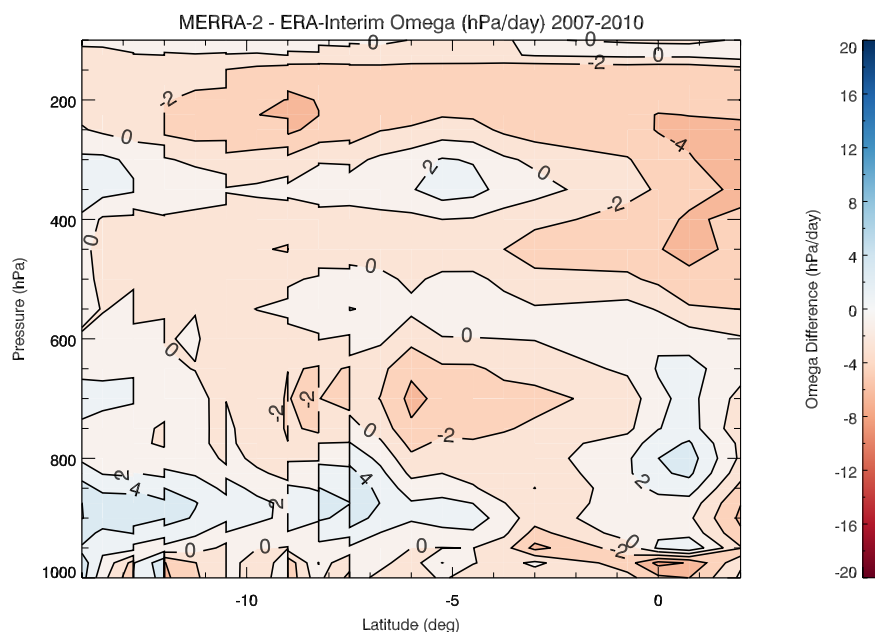
Figure 18. Difference in vertical pressure velocity between MERRA-2 and ERA-Interim.

at these lower latitudes, cumulus clouds are more easily able to penetrate into the free

troposphere and contribute to the breakup of persistent stratocumulus. Analyzing the differences

in specific humidity between MERRA-2 and ERA-Interim, MERRA-2 produces more moisture

at the top of the boundary layer at the beginning of the trajectory at an altitude of about 1000 m.

As the trajectory moves equatorward, MERRA-2 consistently produces higher specific humidity

values than ERA-Interim throughout the majority of the trajectory at low altitudes between 500

and 1000 m. This pattern indicates a possible explanation for the extension of high, vertically-

limited LWC values into near-equatorial latitudes in MERRA-2, as MERRA-2 simulates higher

moisture levels within and at the top of the boundary layer, resulting in more low stratocumulus.

This combined with a strong temperature inversion results in fewer cumulus at lower latitudes

and a subsequent delay in cloud regime shift. Analyzing differences in ω between both

reanalyses throughout the column reveals only small differences in subsidence, with ERA-

Interim producing slightly more subsidence at midlevels. Figure 19 illustrates the relative

relationships between midlevel subsidence produced in each reanalysis, showing that MERRA-2

and ERA-Interim produce essentially equivalent ω_{500} along most of the transition trajectory until

nearing the equator. Figure 19 also highlights the large discrepancy in subsidence between

MERRA and MERRA-2 at high latitudes, with MERRA-2 producing subsidence values more

than 10 hPa/day greater than MERRA, further emphasizing the large differences in dynamical

background conditions between each iteration of MERRA, and possibly explaining why

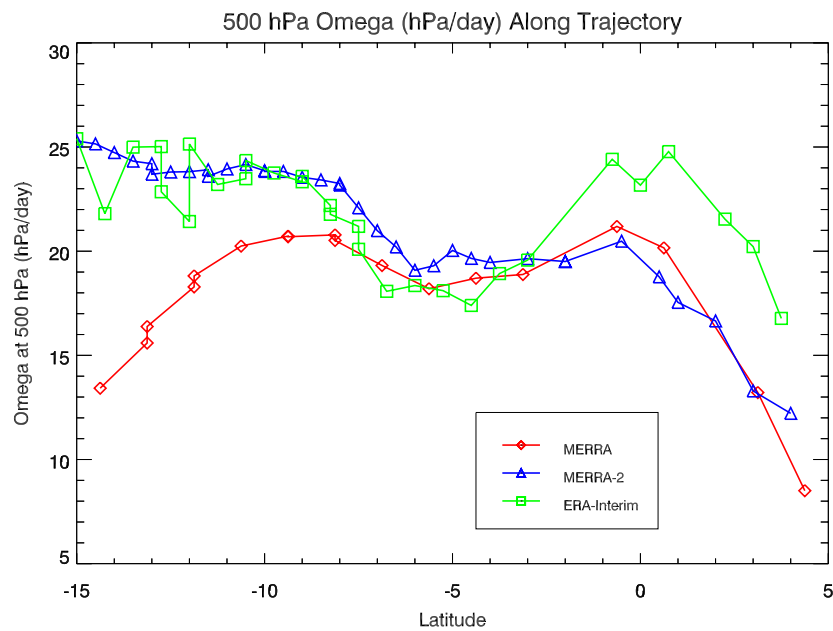MERRA has lower cloud fraction at the beginning of the transition trajectory.

Figure 19. Relative magnitude of atmospheric subsidence along the transition trajectory for each reanalysis, displayed as ω_{500}.

SECTION IV

CONCLUSION

Thorough analysis of three common atmospheric reanalysis datasets has revealed that many differences exist in the simulation of the stratocumulus to cumulus cloud regime transition in the SEP region. Throughout the entire SEP region, each reanalysis simulates different overall areal cloud fraction and varying vertical profiles of cloud liquid water content, implying that underlying internal differences exist between reanalyses in terms of dynamical and thermodynamical variables in the model environment. In general, MERRA-2 has improved upon MERRA in terms of magnitude of overall cloud fraction at the beginning of the trajectory, with higher cloud fraction values in this region implying that MERRA-2 is able to more accurately resolve the features associated with producing and maintaining stratocumulus clouds. ERA-Interim is similar to MERRA-2 in this manner; however, all reanalysis products under-simulate cloud fraction at these higher latitudes compared to observational data. ERA-Interim is also more progressive than both versions of MERRA in simulating the transition from stratocumulus to shallow cumulus as the trajectory moves equatorward, and it simulates a rate of change in cloud fraction similar to the rate seen in observations. Yet, at higher latitudes, ERA-Interim generally under-simulates cloud fraction along the trajectory by approximately 10 to 15% compared to CloudSat observations.

When analyzing the differences in atmospheric state variables between MERRA and MERRA-2, patterns emerge that suggest that MERRA-2 and MERRA are fundamentally different in their simulations of the stratocumulus occurring at the beginning of the trajectory, with much less distinct differences between the two as the trajectory nears the equator. In the

stratocumulus region, MERRA-2 produces a considerably stronger temperature and moisture inversion at the top of the boundary layer than MERRA. In addition, the magnitude of mid-level atmospheric subsidence at higher latitudes is greater in MERRA-2 than in MERRA, with MERRA-2 simulating subsidence on the order of 10 hPa/day greater than MERRA. The improvement in areal cloud fraction representation in MERRA-2 compared to MERRA plus the combination of a stronger temperature and moisture inversion with stronger subsidence implies that accurate representation of both dynamical and thermodynamical variables is important to correctly simulating cloud coverage and regime in reanalysis products, especially in areas dominated by stratocumulus clouds.

While representation of stratocumulus coverage at higher latitudes near the beginning of the transition trajectory is improved in MERRA-2 over MERRA, both iterations of MERRA over-simulate cloud fraction values at lower latitudes in the area of the SEP that is physically known to be dominated by the shallow cumulus cloud regime. MERRA and MERRA-2 therefore likely do not correctly simulate the cloud regime transition process, a conclusion further supported by the lack of significant consistent decrease in cloud fraction along the trajectory that is seen in both ERA-Interim and CloudSat observations. ERA-Interim produces similar cloud fraction values to MERRA-2 at higher latitudes, but seems to be considerably more realistic in simulating the physical process of cloud fraction decrease consistent with cloud regime transition despite its tendency to simulate too few clouds overall.

The comparison of atmospheric state variables between MERRA-2 and ERA-Interim reveals some of the underlying causes for such a different simulation of this transition. While MERRA-2 produces a stronger temperature and moisture inversion than ERA-Interim in the stratocumulus region, comparisons reveal that MERRA-2 continues to simulate this rather strong

inversion for much of the transition trajectory, keeping temperatures warmer above the boundary layer than ERA-Interim, while also keeping the top of the boundary layer moister than ERA-Interim. This suggests that the maintenance of an inversion through much of the trajectory is preventing MERRA-2 from facilitating the destruction of stratocumulus, as the inversion continues to trap moisture at the top of the boundary layer and does not allow for adequate upward vertical growth of cumulus clouds necessary for cloud regime transition. Analysis also reveals that there is little to no difference in atmospheric subsidence values between MERRA-2 and ERA-Interim at lower latitudes, implying that differences in cloud regime transition between these two reanalyses are primarily due to thermodynamical differences between the two reanalysis environments.

This analysis has revealed many interesting characteristics of the stratocumulus to cumulus transition in the SEP region. Most notably, it has been found that some of the most recent and advanced reanalysis products available still inaccurately simulate cloud coverage during the transition from stratocumulus to cumulus regimes by consistently under-producing clouds, in the case of ERA-Interim, or under-producing clouds at higher latitudes and over-producing clouds at lower latitudes, in the case of MERRA and MERRA-2. By comparing the background atmospheric environments within each reanalysis, it was found that stratocumulus production at relatively high latitudes within reanalysis can vary considerably depending on the strength of the temperature and moisture inversion immediately above the top of the boundary layer. Moreover, dynamical effects from the strength of atmospheric subsidence within the background environment also greatly influence stratocumulus prevalence, suggesting that both dynamical and thermodynamical processes are crucial to cloud regime depiction at higher latitudes. At lower latitudes near the equator toward the end of the climatological transition

trajectory, the most notable differences found were between thermodynamical variables, which prevented accurate simulations of the transition into the cumulus cloud regime.

The distinct differences between reanalysis products and observational data detailed in this study and poor representation of the SEP region stratocumulus to cumulus transition also have an overall negative effect on the accuracy of reanalysis radiative products. Cloud radiative forcing at the top of the atmosphere produced by each reanalysis and observed by CloudSat is presented in Figure 20a-b. This metric is useful in illustrating the magnitude of shortwave radiation reflected by clouds and shows how varying amounts of clouds produced by reanalysis
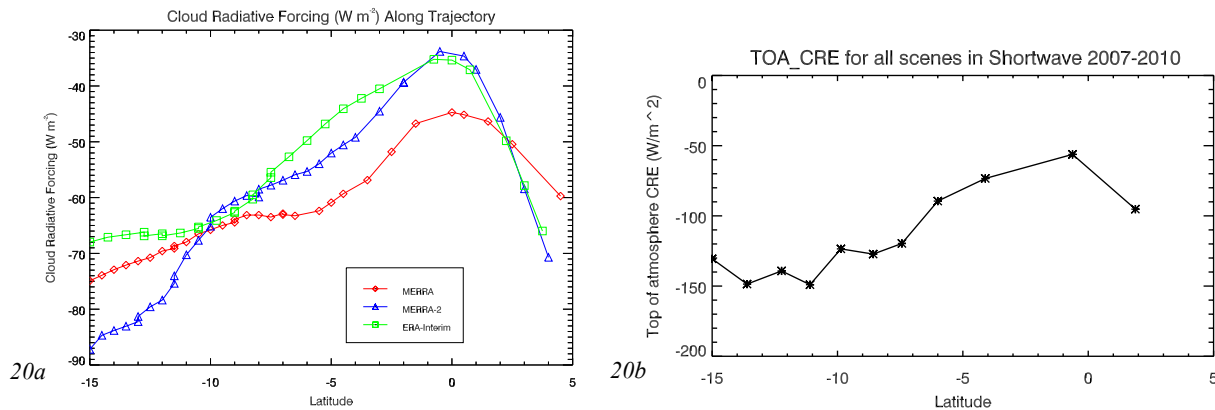

Figure 20. Cloud radiative forcing at the top of the atmosphere produced by each reanalysis (a) and observed by CloudSat (b). Figure 20b from Zapalac 2014.

affect the accuracy of reanalysis radiative products. In general, the cloud radiative forcing observed by CloudSat is significantly greater than all reanalyses at higher latitudes near the beginning of the trajectory. This information, along with knowledge that CloudSat observes more clouds than all reanalyses at these latitudes, illustrates the importance of accurate simulation of clouds within reanalyses. Principally, because all reanalyses produce too few clouds at these higher latitudes, they therefore are unable to produce accurate shortwave radiation budgets due to inaccurate albedo resulting from incorrect cloud simulations. Looking more closely at each reanalysis, ERA-Interim, which was shown to be the most realistic in

reducing cloud fraction and facilitating a transition from shallow stratocumulus to deeper cumulus clouds, produces the weakest, most inaccurate cloud radiative forcing along most of the trajectory. This is due to ERA-Interim producing too few clouds throughout the SEP region, further emphasizing the importance of accurate simulation of clouds within reanalysis.

While all reanalysis products analyzed in this study exhibit significant shortcomings in accurately simulating cloud regime transition, future improvements in modeling thermodynamical variables at low levels along known transition trajectories will likely result in more accurate simulations of overall cloud fraction. This in turn will aid in improving overall outgoing radiation values produced by reanalysis, which will contribute to a better understanding of the cloud-related controls and processes governing the global energy cycle.

REFERENCES

Bony, S., and J.L. Dufresne, 2005: Marine boundary layer clouds at the heart of tropical cloud feedback uncertainties in climate models. *Geophysical Research Letters*, **32**, L20806, DOI: 10.1029/2005GL023851.

Bretherton, C.S., and M.C. Wyant, 1997: Moisture transport, lower-tropospheric stability, and decoupling of cloud-topped boundary layers. *J. Atmos. Sci.,* **54**, 148-167, DOI: 10.1175/1520-0469(1997)054<0148:MTLTSA>2.0.CO;2.

Brooks, M.E., R.J. Hogan, and A.J. Illingworth, 2005: Parameterizing the difference in cloud fraction defined by area and by volume as observed with radar and lidar. *J. Atmos. Sci.*, **62**, 2248-2260, DOI: 10.1175/JAS3467.1.

Chen, T., W.B. Rossow, and Y.C. Zhang, 2000: Radiative effects of cloud-type variations. *J. Climate*, **13**, 264-286, DOI: 10.1175/1520-0442(2000)013<0264:REOCTV>2.0.CO;2.

Dee, D. P., and Coauthors, 2011: The ERA-Interim reanalysis: configuration and performance of the data assimilation system. *Quarterly Journal of the Royal Meteorological Society*, **137**, 553-597, DOI: 10.1002/qj.828.

Duynkerke, P.G., and J. Teixeira, 2001: Comparison of the ECMWF reanalysis with FIRE I observations: Diurnal variation of marine stratocumulus. *J. Climate*, **14**, 1466-1478, DOI: 10.1175/1520-0442(2001)014<1466:COTERW>2.0.CO;2.

Gelaro, R., and Coauthors, 2017: The Modern-Era Retrospective Analysis for Research and Applications, Version 2 (MERRA-2). *J. Climate*, **30**, 5419-5454, DOI: 10.1175/JCLI-D-16-0758.1.

Hahn, C. J., W. B. Rossow, and S. G. Warren, 2001: IS-CCP cloud properties associated with standard cloud types identified in individual surface observations. *J. Climate,* **14**, 11–28, DOI: 10.1175/1520-0442(2001)014<0011:ICPAWS>2.0.CO;2.

Jakob, C., 1999: Cloud cover in the ECMWF reanalysis. *J. Climate*, **12**, 947-959, DOI: 10.1175/1520-0442(1999)012<0947:CCITER>2.0.CO;2.

Klein, S.A., and D.L. Hartmann, 1993: The seasonal cycle of low stratiform clouds. *J. Climate,* **6**, 1587-1606, DOI: 10.1175/1520-0442(1993)006<1587:TSCOLS>2.0.CO;2.

Rienecker, M. M., and Coauthors, 2011: MERRA:NASA's Modern-Era Retrospective Analysis for Research and Applications. *J. Climate*, **24**, 3624-3648, DOI: 10.1175/JCLI-D-11-00015.1.

Sandu, I., B. Stevens, and R. Pincus, 2010: On the transitions in marine boundary layer cloudiness. *Atmospheric Chemistry and Physics,* **10**, 2377-2391, DOI: 10.5194/acp-10-2377-2010.

Siebesma, A.P., and Coauthors, 2004: Cloud representation in general-circulation models over the northern Pacific Ocean: A EUROCS intercomparison study. *Quarterly Journal of the Royal Meteorological Society*, **130**, 3245-3267, DOI: 10.1256/qj.03.146.

Stephens, G.L., and Coauthors, 2002: The CloudSat mission and the A-Train – A new dimension of space-based observations of clouds and precipitation. *Bull. Amer. Meteorol. Soc.,* **83**, 1771-1790, DOI: 10.1175/BAMS-83-12-1771.

Stephens, G.L., and Coauthors, 2008: CloudSat mission: Performance and early science after the first year of operation. *Journal of Geophysical Research-Atmospheres,* **113**, DOI: 10.1029/2008JD009982.

Teixeira, J., and Coauthors, 2011: Tropical and Subtropical Cloud Transitions in Weather and Climate Prediction Models: The GCSS/WGNE Pacific Cross-Section Intercomparison (GPCI). *J. Climate,* **24**, 5223-5256, DOI: 10.1175/2011JCLI3672.1.

Warren, S. G., C. J. Hahn, J. London, R. M. Chervin, and R. L. Jenne, 1986: Global distribution of total cloud cover and cloud types over land. NCAR Technical Note NCAR/TN-273+STR 29pp+200 maps, National Center for Atmospheric Research, Boulder, CO.

Wood, R., and C.S. Bretherton, 2004: Boundary Layer Depth, Entrainment, and Decoupling in the Cloud-Capped Subtropical and Tropical Marine Boundary Layer. *J. Climate,* **17**, 3576-3588, DOI: 10.1175/1520-0442(2004)017<3576:BLDEAD>2.0.CO;2.

Wood, R., 2012: Stratocumulus Clouds. *Monthly Weather Review,* **140**, 2373-2423, DOI: 10.1175/MWR-D-11-00121.1.

Wyant, M. C., C. S. Bretherton, H. A. Rand, and D. E. Stevens, 1997: Numerical simulations and a conceptual model of the stratocumulus to trade cumulus transition. *J. Atmos. Sci.,* **54**, 168–192, DOI: 10.1175/1520-0469(1997)054<0168:NSAACM>2.0.CO;2.

Zapalac, A., 2014: Characteristics of a Marine Stratocumulus to Cumulus Cloud Transition. M.S. Thesis, Dept. of Atmospheric Sciences, Texas A&M University, 93 pp.